International Journal of Modern Physics C
Vol. 17, No. 5 (2006) 631–643

World Scientific
www.worldscientific.com

THERMAL CURVED BOUNDARY TREATMENT FOR THE THERMAL LATTICE BOLTZMANN EQUATION

HAIBO HUANG*, T. S. LEE and C. SHU
Department of Mechanical Engineering
National University of Singapore, Singapore
10 Kent Ridge Crescent, Singapore 119260
**g0301108@nus.edu.sg*

Received 17 November 2005
Revised 28 November 2005

In this paper, a recent curved non-slip wall boundary treatment for isothermal Lattice Boltzmann equation (LBE) [Z. Guo, C. Zheng and B. Shi, *Phys. Fluids* **14**(6) (2002)] is extended to handle the thermal curved wall boundary for a double-population thermal lattice Boltzmann equation (TLBE). The unknown distribution population at a wall node which is necessary to fulfill streaming step is decomposed into its equilibrium and non-equilibrium parts. The equilibrium part is evaluated according to Dirichlet and Neumann boundary constraints, and the non-equilibrium part is obtained using a first-order extrapolation from fluid lattices. To validate the thermal boundary condition treatment, we carry out numerical simulations of Couette flow between two circular cylinders, the natural convection in a square cavity, and the natural convection in a concentric annulus between an outer square cylinder and an inner circular cylinder. The results agree very well with analytical solution or available data in the literature. Our numerical results also demonstrate that the TLBE together with the present boundary scheme is of second-order accuracy.

Keywords: Lattice Boltzmann; thermal; curved boundary.

1. Introduction

The lattice Boltzmann method (LBM) has been proposed as an alternative numerical scheme for solving the incompressible Navier–Stokes (NS) equations.[1–4] In LBM, the boundary conditions treatments are important for obtaining accurate results. There are many non-slip wall boundary treatments for isothermal flows, for example, the bounce-back scheme,[5] the half-way bounce-back scheme,[6] the hydrodynamic approach,[7] the non-equilibrium bounce-back scheme[8] and the extrapolation scheme,[9] and so on. To handle curved wall boundary conditions more accurately, Fillipova and Hänel,[10] and later Mei *et al.*[11] improved the bounce-back rule for curved boundary. Later, a much simple and accurate boundary treatment combining bounce-back scheme and interpolation was proposed by Bouzidi *et al.*[12] Guo *et al.*[13] also proposed non-equilibrium distribution extrapolation method for

non-slip curved wall boundary condition. Using the above boundary condition treatments for isothermal fluid flow problem is very successful.[12,13]

On the other hand, to simulate heat transfer phenomena, effort of establishing a satisfactory thermal LBE models is ongoing.[14–16] In general, the present thermal lattice Boltzmann models can be classified into three categories: the multispeed approach,[14] the passive-scalar approach, and the double-population approach. In the multispeed approach,[14] the internal energy term is incorporated with a density distribution function so that only the density distribution function is needed, however, these multi-speed models suffer severe numerical instability, and the temperature variation is limited to a narrow range.[16] To enhance numerical stability, a separate distribution function which is independent of the density distribution is proposed in the passive-scalar thermal LBE model.[15] However, the viscous heat dissipation and compression work done by the pressure cannot be taken into account.[16] In the third approach,[16] the temperature field is obtained through an independent internal energy density distribution function. The model has better numerical stability and the viscous heat dissipation and compression work done by the pressure can be solved fundamentally.

At the same time, constructing stable thermal boundary treatment for TLBE models is also in progress.[16–20] He *et al.*[16] applied the bounce-back rule of the non-equilibrium distribution to the thermal boundary distribution. Tang *et al.*[17] adopt local thermal equilibrium distribution functions on wall nodes for unknown populations. D' Orazio *et al.*[18] applied a "counter-slip" approach[19] to handle the thermal boundary condition. Although the scheme of assuming a counter slip thermal energy density achieved high accuracy,[18] the counter-temperature assumption may cast doubt on its convenient applicability to arbitrary boundary conditions or complicated geometries.[3,9]

Here, based on the idea of Guo *et al.*,[13] for uniform regular lattices, we introduce a thermal curved boundary condition for the doubled-population TLBE model. The distribution at a wall node was decomposed into two parts, i.e., the equilibrium part and the non-equilibrium one. The nonequilibrium part is approximated by that of the neighboring fluid node along the link, and the equilibrium part is determined by a fictitious equilibrium distribution where the boundary condition is enforced.[13]

The outline of this paper is as follows: In Sec. 2, a brief description of the double-population approach TLBE[16] is given. In Sec. 3, the thermal boundary conditions for arbitrary curved wall were derived. In Sec. 4, some numerical solutions valid the boundary treatment and finally we conclude the paper.

2. Thermal LBE Model

In our study, a double-population TLBE derived by He *et al.*[16] is used. The two discrete evolution equations in the TLBE are Eqs. (1) and (2),

$$\overline{f_i}(\mathbf{x}+\mathbf{e}_i\delta t, t+\delta t) - \overline{f_i}(\mathbf{x},t)$$
$$= -\frac{\delta t}{\tau_f + 0.5\delta t}[\overline{f_i}(\mathbf{x},t) - f_i^{\mathrm{eq}}(\mathbf{x},t)] + \frac{\tau_f \delta t}{\tau_f + 0.5\delta t} F_i \,, \tag{1}$$

$$\overline{g_i}(\mathbf{x}+\mathbf{e}_i\delta t, t+\delta t) - \overline{g_i}(\mathbf{x},t)$$
$$= -\frac{\delta t}{\tau_g + 0.5\delta t}[\overline{g_i}(\mathbf{x},t) - g_i^{\mathrm{eq}}(\mathbf{x},t)] - \frac{\tau_g \delta t}{\tau_g + 0.5\delta t} f_i(\mathbf{x},t) q_i \,. \tag{2}$$

Where, the new variables $\bar{f}$ and $\bar{g}$ are defined as

$$\overline{f_i} = f_i + \frac{0.5\delta t}{\tau_f}(f_i - f_i^{\mathrm{eq}}) - \frac{\delta t}{2} F_i \,, \tag{3}$$

$$\overline{g_i} = g_i + \frac{0.5\delta t}{\tau_g}(g_i - g_i^{\mathrm{eq}}) + \frac{\delta t}{2} f_i q_i \,, \tag{4}$$

$$F_i = \frac{\mathbf{G}(\mathbf{e}_i - \mathbf{u})}{RT} f_i^{\mathrm{eq}} \,, \tag{5}$$

$$q_i = (\mathbf{e}_i - \mathbf{u}) \left[\frac{\partial \mathbf{u}}{\partial t} + (\mathbf{e}_i \cdot \nabla)\mathbf{u} \right] . \tag{6}$$

where $f(\mathbf{x},t)$ and $g(\mathbf{x},t)$ are the density distribution function and the thermal energy density distribution function in position $\mathbf{x}$ at time t respectively. τ_f and τ_g are the momentum and internal energy relax time, respectively. In Eq. (5), $\mathbf{G}$ are the external forces acting on unit mass. $\mathbf{e}_i$ is the lattice velocity and i denotes the velocity direction. δx, δt and are the lattice spacing and time step size. Equation (6) represents the effect of viscous heating and it can be expressed as[19]

$$q_i = (\mathbf{e}_i - \mathbf{u}) \frac{[\mathbf{u}(\mathbf{x}+\mathbf{e}_i\delta t, t+\delta t) - \mathbf{u}(\mathbf{x},t)]}{\delta t} \,. \tag{7}$$

For D2Q9 model, the 9 discrete velocities are as following, the direction can also refer to Fig. 1,

$$\mathbf{e}_i = \begin{cases} (0,0) & i = 0 \\ \left(\cos\left[(i-1)\dfrac{\pi}{2}\right], \sin\left[(i-1)\dfrac{\pi}{2}\right]\right) c & i = 1,2,3,4 \\ \sqrt{2}\left(\cos\left[(i-5)\dfrac{\pi}{2} + \dfrac{\pi}{4}\right], \sin\left[(i-5)\dfrac{\pi}{2} + \dfrac{\pi}{4}\right]\right) c & i = 5,6,7,8 \end{cases} . \tag{8}$$

In above expression, $c = \delta x/\delta t = \sqrt{3RT_0}$, T_0 is the average temperature. In this paper $c = 1$ and $\delta t = \delta x = 1$.

In above Eqs. (1)–(5), f_i^{eq}, g_i^{eq} are the equilibrium density distribution functions and equilibrium internal energy distribution functions respectively. They are defined as,[16]

$$f_i^{\mathrm{eq}}(\mathbf{x},t) = \omega_i \rho \left[1 + \frac{\mathbf{e}_i \cdot \mathbf{u}}{c_s^2} + \frac{(\mathbf{e}_i \cdot \mathbf{u})^2}{2c_s^4} - \frac{\mathbf{u}^2}{2c_s^2} \right] , \quad i = 0,1,2,\ldots,8 \,, \tag{9}$$

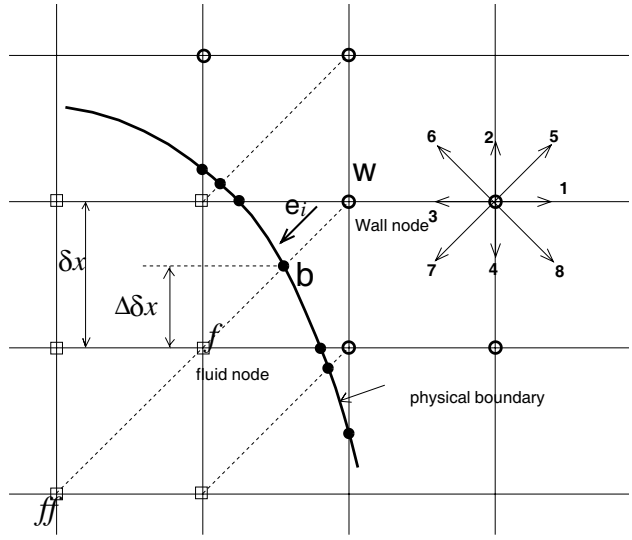

Fig. 1. Curved boundary and lattice nodes (open circle is wall nodes, open square is fluid nodes, filled circle is the physical boundary nodes in the link of fluid node and wall node).

$$g_0^{\mathrm{eq}}(\mathbf{x},t) = \omega_i \rho e \left(-\frac{3\mathbf{u}^2}{2c^2}\right), \tag{10}$$

$$g_i^{\mathrm{eq}}(\mathbf{x},t) = \omega_i \rho e \left[\frac{3}{2} + \frac{3(\mathbf{e}_i\cdot\mathbf{u})}{2c^2} + \frac{9(\mathbf{e}_i\cdot\mathbf{u})^2}{2c^4} - \frac{3\mathbf{u}^2}{2c^2}\right], \quad i = 1,2,3,4, \tag{11}$$

$$g_i^{\mathrm{eq}}(\mathbf{x},t) = \omega_i \rho e \left[3 + \frac{6(\mathbf{e}_i\cdot\mathbf{u})}{c^2} + \frac{9(\mathbf{e}_i\cdot\mathbf{u})^2}{2c^4} - \frac{3\mathbf{u}^2}{2c^2}\right], \quad i = 5,6,7,8, \tag{12}$$

where $c_s = c/\sqrt{3}$, $\omega_0 = 4/9$, $\omega_i = 1/9$, $(i = 1, 2, 3, 4)$, $\omega_i = 1/36$, $(i = 5, 6, 7, 8)$. The internal energy density is $\rho e = \rho RT$ for two-dimensional problems.

Finally, the macroscopic density ρ and momentum $\rho\mathbf{u}$, internal energy per unit mass e, heat flux $\mathbf{q}$, which is a vector different from q_i in Eq. (6) or (7), kinetic viscosity ν and thermal diffusivity α are obtained by[16,19]

$$\rho = \sum_{i=0}^{8} \overline{f_i}, \qquad \rho\mathbf{u} = \sum_{i=0}^{8} \overline{f_i}\mathbf{e}_i + \frac{\rho\mathbf{G}\delta t}{2}, \tag{13}$$

$$\rho e = \sum_{i=0}^{8} \overline{g_i} - \frac{\delta t}{2}\sum_i f_i q_i, \tag{14}$$

$$\mathbf{q} = \left(\sum_{i=0}^{8} \mathbf{e}_i\overline{g_i} - \rho e\mathbf{u} - \frac{\delta t}{2}\sum_{i=0}^{8}\mathbf{e}_i f_i q_i\right)\frac{\tau_g}{\tau_g + 0.5\delta t}, \tag{15}$$

$$\nu = \tau_f RT_0 \quad \text{and} \quad \alpha = 2\tau_g RT_0. \tag{16}$$

3. Boundary Condition

The curved non-slip wall boundary treatment[13] is applied for velocity boundary conditions in this paper and now, the treatment is extended to handle the thermal curved wall boundary for a double-population thermal lattice Boltzmann equation (TLBE). Basically, to evaluate internal energy density distribution functions, the two main steps of TLBE model are collision and streaming. In the collision step, the post-collision distribution function obtained by

$$\overline{g_i}^{+}(\mathbf{x},t) = (1-\omega_g)\overline{g_i}(\mathbf{x},t) + \omega_g g_i^{\mathrm{eq}}(\mathbf{x},t) - \omega_g \tau_g f_i q_i \,, \tag{17}$$

where $\omega_g = \delta t/(\tau_g + 0.5\delta t)$. In the streaming step, the distribution functions of new time level is

$$\overline{g_i}(\mathbf{x} + \mathbf{e}_i\delta t, t + \delta t) = \overline{g_i}^{+}(\mathbf{x},t)\,. \tag{18}$$

However, to fulfill the streaming step, some unknown internal energy density distribution functions should be determined. For example, in Fig. 1, it is obvious that to fulfill the streaming step, some unknown $\overline{g_i}^{+}(\mathbf{x}_w,t)$ ($i = 3, 7$) in wall nodes $\mathbf{x}_w$ need to be specified. To specify $\overline{g_i}^{+}(\mathbf{x}_w,t)$, In Eq. (17) the term $\overline{g_i}(\mathbf{x}_w,t)$ can be decomposed into two parts,[13]

$$\overline{g_i}(\mathbf{x}_w,t) = g_i^{\mathrm{eq}}(\mathbf{x}_w,t) + g_i^{ne}(\mathbf{x}_w,t) \tag{19}$$

where $g_i^{\mathrm{eq}}(\mathbf{x}_w,t)$ and $g_i^{ne}(\mathbf{x}_w,t)$ are the equilibrium and nonequilibrium part of $\overline{g_i}(\mathbf{x}_w,t)$.

Firstly, we discuss how to determine the equilibrium part $g_i^{\mathrm{eq}}(\mathbf{x}_w,t)$. Equations (10)–(12) illustrated that once $\rho(\mathbf{x}_w)$, $T(\mathbf{x}_w)$, $\mathbf{u}(\mathbf{x}_w)$ is known, then $g_i^{\mathrm{eq}}(\mathbf{x}_w,t)$ can be determined. Here, for simplicity, ρ_w, T_w, $\mathbf{u}_w$ are used to denote $\rho(\mathbf{x}_w)$, $T(\mathbf{x}_w)$, $\mathbf{u}(\mathbf{x}_w)$, the macro variables in other lattice nodes are written in this way. Here, ρ_w is specified as $\rho_w = \rho(\mathbf{x}_w + \mathbf{e}_i) = \rho_f$. T_w is determined by linear extrapolation using either $T_{w1} = (T_b + (\Delta - 1)T_f)/\Delta$ or $T_{w2} = (2T_b + (\Delta - 1)T_{ff})/(1 + \Delta)$. Where Δ is the fraction of the intersected link in the fluid region $\Delta = |\mathbf{x}_f - \mathbf{x}_b|/|\mathbf{x}_f - \mathbf{x}_w|$, which is illustrated in Fig. 1. Usually, T_{w1} can be used as a good approximation for T_w for $\Delta > 0.75$, However, if Δ is small, using T_{w1} to evaluate T_w may cause instability. Alternative, for $\Delta < 0.75$ we used $T_w = \Delta T_{w1} + (1 - \Delta)T_{w2}$. The extrapolation scheme is the same as Ref. 13.

Next, to determine the $g_i^{ne}(\mathbf{x}_w,t)$, extrapolation method is also used. $g_i^{ne}(\mathbf{x}_w,t)$ is evaluated as $g_i^{ne}(\mathbf{x}_w,t) = \Delta g_i^{ne}(\mathbf{x}_f,t) + (1-\Delta)g_i^{ne}(\mathbf{x}_{ff},t)$. From the Chapman-Enskog analysis,[16] $g_i^{ne}(\mathbf{x}_w,t)$ can be expressed as $g_i^{ne} = g_i^{(1)}\delta x$, where $g_i^{(1)}$ is of the same order as g_i^{eq}. Since $g_i^{(1)}(\mathbf{x}_w,t) - g_i^{(1)}(\mathbf{x}_f,t) = O(\delta x)$, $g_i^{ne}(\mathbf{x}_w,t) - g_i^{ne}(\mathbf{x}_f,t) = O(\delta x^2)$. For lattice node $\mathbf{x}_{ff}$, the accuracy analysis is the same as above. That means the approximation $g_i^{ne}(\mathbf{x}_w,t)$ is of second order in space which is in consistent with TLBE.

Finally, the thermal curved boundary treatment to specify $\overline{g_i}^{+}(\mathbf{x}_w,t)$ is

$$\overline{g_i}^{+}(\mathbf{x}_w,t) = g_i^{\mathrm{eq}}(\mathbf{x}_w,t) + (1-\omega_g)g_i^{ne}(\mathbf{x}_w,t) - \omega_g\tau_g f_i q_i \,. \tag{20}$$

Since the Neumann curved wall boundary can be transferred into Dirichlet boundary condition, then the above Dirichlet curved wall boundary treatment can also be applied to Neumann curved wall boundary. As an example, we consider the same wall node "w" in the Fig. 1. Once the heat flux (temperature gradient $(\partial T/\partial n)$ at "b" is given, $\mathbf{n}$ is the unit vector normal to the local wall and pointing to fluid region. $(\partial T/\partial n)_i$ is used to represent the temperature gradient in $\mathbf{e}_i$ direction. That is $(\partial T/\partial n)_i = (\partial T/\partial n)\mathbf{e}_i\mathbf{n}/|\mathbf{e}_i|$. Using Taylor series expansion, with second order accuracy in space, the temperature on node "w" can be approximated by:

$$T_w = \frac{1}{3}\left(4T_f - T_{ff} - 2\left(\frac{\partial T}{\partial n}\right)_i |e_i|\delta t\right). \tag{21}$$

Hence, after the equilibrium part is evaluated according to Dirichlet and Neumann boundary constraints, and the non-equilibrium part is obtained using a first-order extrapolation from fluid lattices, $\overline{g_i}^+(\mathbf{x}_w, t)$ is obtained to fulfill the streaming step.

4. Results and Discussion

4.1. *Couette flow between two circular cylinders*

To demonstrate the capability of the present thermal curved wall boundary treatment and investigate its spatial accuracy, the Couette flow between two circular cylinders is simulated. In this flow, the inner cylinder with radius r_1 rotates with a constant tangent velocity u_0 ($u_0 = \omega r_1$, ω is the angular velocity) and the outer cylinder with radius r_2 is kept stationary. The temperature of inner cylinder is kept as T_1 and that of outer cylinder is kept T_2. This Couette flow has the following analytical solution,

$$u_\theta(r) = C\left(\frac{r_2}{r_1} - \frac{r}{r_2}\right), \tag{22}$$

$$T_\theta(r) = \frac{\Pr C^2 r_2^2}{r^2} + \frac{\Pr C^2(1/\eta^2 - 1) + (T_1 - T_2)}{\ln \eta}\ln\left(\frac{r}{r_2}\right) + T_2 + \Pr C^2, \tag{23}$$

where $C = u_0\eta(1-\eta^2)$, $\eta = r_1/r_2$, the Prandtl number $Pr = \nu/\alpha$, ν is the kinetic viscosity and α is the thermal diffusivity.

In simulations, a uniform square mesh is used to cover the flow domain. The present thermal boundary treatment is applied to the surfaces of the outer and inner cylinders. Firstly, cases of $\mathrm{Re} = (r_2 - r_1)u_0/\nu = 10$ with different values of η are conducted. In these cases $\tau_f = 0.1$, $\tau_g = 0.1$, $r_2 = 40$, and r_1 changes according to r_2 and η. The temperature profiles are plotted together with the analytical ones in Fig. 2. The excellent agreement between the TLBM and the analytical solutions demonstrates the reliability of the present boundary treatment.

Spatial accuracy of the treatment is also tested for cases of $\mathrm{Re} = 10$ and 30. In these cases, $\tau_f = 0.1$, $\tau_g = 0.1$ and $\eta = 0.5$. r_1 changes from 8 to 64, and r_2 changes according to η and r_1. The relative global L_2 norm errors in the temperature field

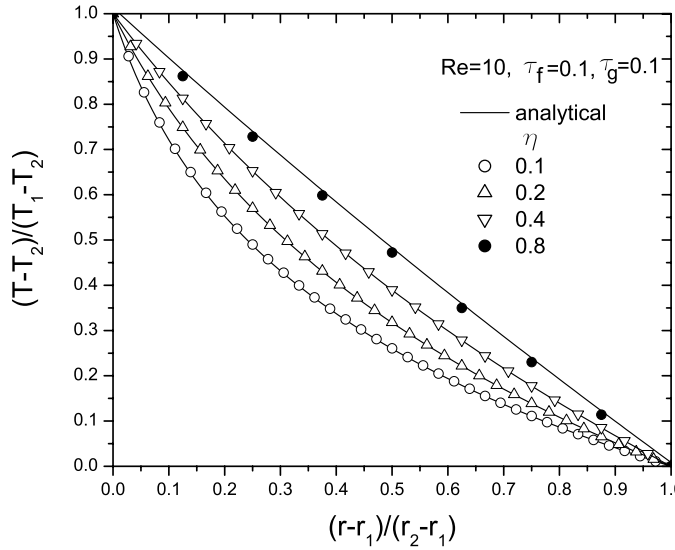

Fig. 2. Temperature profiles of the Couette flow at Re = 10 with difference value of the radius ratio.

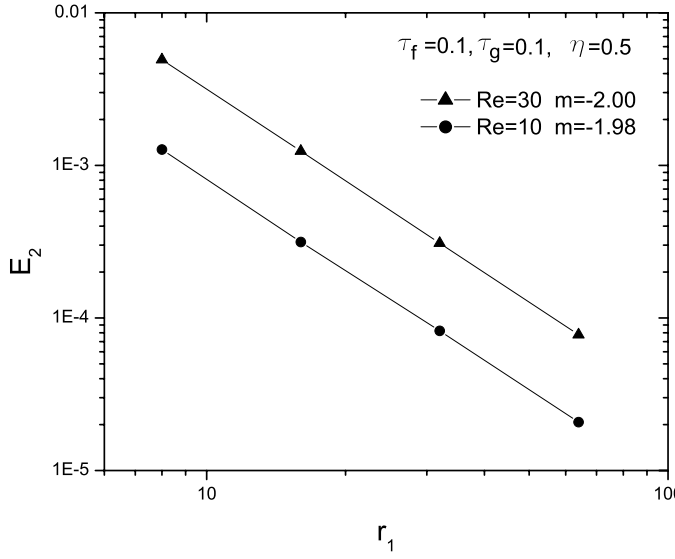

Fig. 3. Temperature relative global errors versus the radius of the inner cylinder in the Couette flow. (m is the slope of linear fitting line).

E_2 are measured and shown in Fig. 3. In Fig. 3, the slopes of the linear fitting lines for Re = 10 and 30 are -1.98 and -2.00 respectively. The slopes are all very close to -2, which confirmed the thermal curved wall treatment is second-order accuracy.

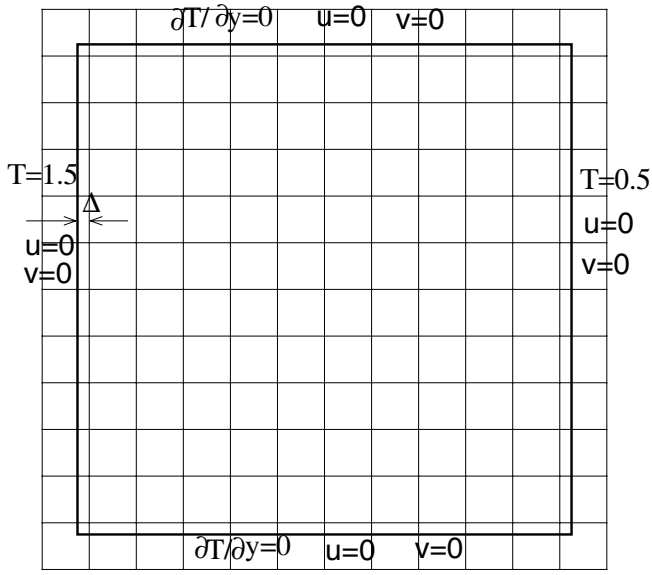

Fig. 4. Boundary condition and geometry of natural convection in a square cavity ($N = 13$).

4.2. *Natural convection in a square cavity*

In order to further validate the thermal boundary treatment, a natural convection in a two-dimensional square cavity is investigated. The temperature difference between the left and right walls introduces a temperature gradient in the fluid, which induces the natural convection in the cavity. The top and bottom walls are adiabatic. The definition of Δ and the boundary conditions are illustrated in Fig. 4. Here to test the thermal boundary treatment, $\Delta = 0.25, 0.5, 0.75$ were studied. The actual size of the cavity is $L \times L = (N - 3 + 2\Delta) \times (N - 3 + 2\Delta)$. N is the total lattice nodes in each spatial direction.

The Boussinesq approximation is applied to the buoyancy force term. This means that the properties β and ν are considered as constants, and the buoyancy term is assumed to depend linearly on the temperature, $\rho\mathbf{G} = \rho\beta g_0(T - T_0)\mathbf{j}$, where β is the thermal expansion coefficient, g_0 is the acceleration due to gravity, T_0 is the average temperature, here it is 1.0, and $\mathbf{j}$ is the vertical direction opposite to that of gravity.

The dynamical similarity depends on two dimensionless parameters: the Prandtl number Pr and the Rayleigh number Ra defined as

$$\mathrm{Pr} = \frac{\nu}{\alpha}\,, \tag{24}$$

$$Ra = \beta g_0 \frac{(T_1 - T_2)L^3}{\nu\alpha}\,. \tag{25}$$

In our simulations, $\mathrm{Pr} = 0.7$. The value of characteristic velocity $U_c = \sqrt{\beta g_0(T_1 - T_2)L}$ was chosen 0.1 for $Ra \leq 10^5$ and 0.15 for $Ra > 10^5$. When U_c is

determined, the kinetic viscosity ν and the thermal diffusivity α can be determined by the two dimensionless numbers Pr and Ra through Eqs. (24) and (25). And then by Eq. (16), two relaxation times τ_f, τ_g, are determined. Another characteristic velocity $U_\infty = \alpha/L$ is also used to normalize velocity and stream functions.

The Nusselt number is one of the most important dimensionless parameters in describing the convective heat transport. The average Nusselt number in the whole flow domain is defined by

$$Nu_a = \frac{L}{\alpha(T_1 - T_2)} \int_0^L \int_0^L q_x(x, y) dx dy \,, \tag{26}$$

where q_x is the heat flux in x direction.

Firstly, the grid-dependence study listed in Table 1, the data taken from cases of $\Delta = 0$, $Ra = 10^4$. The grid size is taken as $N \times N$, where N is the total lattice nodes in each spatial direction. Table 1 shows the numerical results of normalized $u_{\max}$ on the vertical midplane of the cavity and corresponding position y, normalized $v_{\max}$ on the horizontal midplane and corresponding position x, and Nu_a. When grid size becomes larger, our results are more close to the benchmark solutions in Ref. 21. Grid size 103×103 is fine enough to obtain accurate results. Hence in the studies of other cases, the grid size used is 103×103.

Table 2 shows the numerical results of cases with $\Delta = 0.5$ (actual size of the cavity is 101×101) for a wide range of Rayleigh numbers. The benchmark numerical solution using the differential quadrature (DQ) method[21] are also listed for comparison. It can be seen from Table 2 that, our numerical results agree very well with

Table 1. Grid-dependence study for the natural convection in a square cavity at $Ra = 10^4$, $\Delta = 0$.

Mesh	53×53	103×103	153×153	DQ[21]
$u_{\max}$	15.980	16.133	16.133	16.190
y	0.818	0.819	0.823	0.825
$v_{\max}$	19.390	19.580	19.580	19.638
x	0.121	0.120	0.120	0.120
Nu_a	2.225	2.241	2.244	2.245

Table 2. Numerical results for cases with $\Delta = 0.5$, $Ra = 10^3$–10^6.

	10^3		10^4		10^5		10^6	
Ra	TLBE	Ref. 21	TLBE	Ref. 21	TLBE	Ref. 21	TLBE	Ref. 21
$u_{\max}$	3.652	3.649	16.197	16.190	34.844	34.736	64.872	64.775
y	0.817	0.815	0.827	0.825	0.856	0.855	0.847	0.850
$v_{\max}$	3.705	3.698	19.613	19.638	68.582	68.640	219.18	220.64
x	0.173	0.180	0.124	0.120	0.064	0.065	0.035	0.035
Nu_a	1.118	1.118	2.243	2.245	4.512	4.523	8.729	8.762

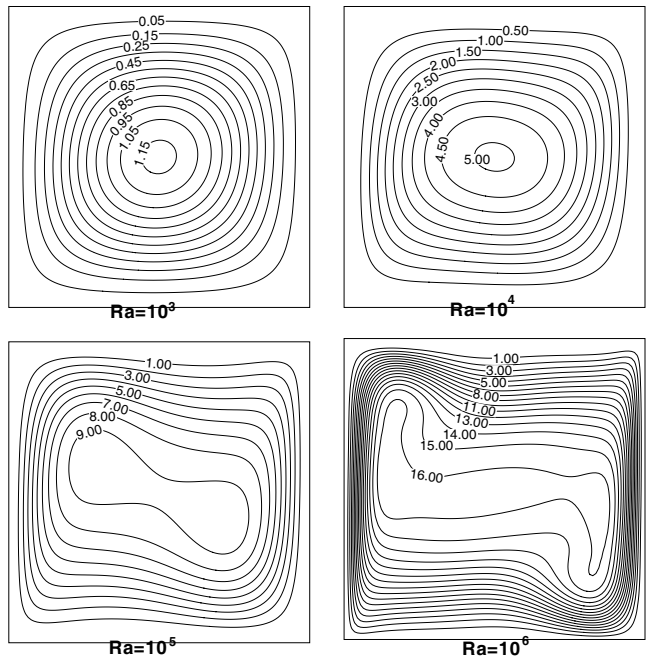

Fig. 5. Streamlines of natural convection at $Ra = 10^3$, 10^4, 10^5, 10^6 for cases $\Delta = 0.5$.

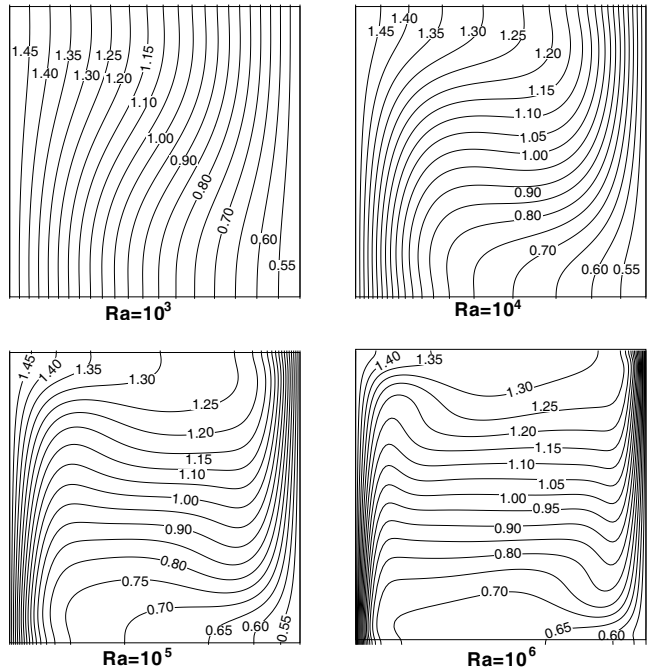

Fig. 6. Isotherms of natural convection at $Ra = 10^3$, 10^4, 10^5, 10^6 for cases $\Delta = 0.5$.

Table 3. Numerical results for $Ra = 10^4$ with mesh size 103×103 and different Δ.

Mesh	$\Delta = 0$	$\Delta = 0.25$	$\Delta = 0.5$	$\Delta = 0.75$	DQ[21]
$u_{\max}$	16.133	16.218	16.197	16.173	16.190
y	0.819	0.828	0.827	0.825	0.825
$v_{\max}$	19.580	19.652	19.613	19.600	19.638
x	0.120	0.122	0.124	0.116	0.120
Nu_a	2.241	2.240	2.243	2.239	2.245

that of Ref. 21. With the increase of the Rayleigh number, due to the enhancement of natural convection, normalized $u_{\max}$, normalized $v_{\max}$, Nu_a are increased greatly, and the position of maximum vertical velocity on the horizontal midplane moves closer to the wall. Figure 5 and 6 show the contour of normalized stream function and isotherms of $Ra = 10^3$, 10^4, 10^5, 10^6. These plots all agree well with Ref. 21.

To investigate the effect of different Δ, cases with $\Delta = 0$, 0.25, 0.5, 0.75 for $Ra = 10^4$ were simulated. The results are illustrated in Table 3. It can be seen from Table 3 that for different Δ, TLBE with present thermal boundary treatment can all give out very accurate results.

4.3. *Natural convection in a concentric annulus between an outer square cylinder and an inner circular cylinder*

The natural convection in a concentric annulus between an outer square cylinder and an inner circular cylinder were investigated for Rayleigh numbers 10^4, 5×10^4 and 10^5. The geometry ratio between the square cylinder and circular cylinder is defined as $\eta = 2r_i/L$ and is fixed at 0.4 in our simulation. The temperatures of inner cylinder and outer square are fix as 2.5, 1.5 respectively. Here in our simulations the grid size is 103×103. The Prandtl number $\mathrm{Pr} = 0.71$ and $U_c = \sqrt{\beta g_0 (T_1 - T_2) L} = 0.1$. Equations (24) and (25) are also used to determine the kinetic viscosity ν and the thermal diffusivity α.

The non-dimensional stream function is defined as $\psi = \psi^*/LU_\infty$, ψ^* is dimensional stream function and $U_\infty = \alpha/L$, The contours of non-dimensional stream functions in the annulus at $Ra = 10^4$, 5×10^4, 10^5 are shown in Fig. 7. The streamline of $\psi = 0$ is almost in the vertical midplane and the contours are symmetric with respect to vertical midplane. The isotherms in the annulus are shown in Fig. 8, the contours are also symmetric with respect to the vertical midplane. Figures 7 and 8. are all in good agreement with the plots shown in Refs. 22 and 23.

Since in the steady state, the Nusselt numbers along the inner and outer walls are the same, there is no need to pay separate attentions to the average Nusselt numbers for the outer and inner boundaries. The average Nusselt number on the inner cylinder or outer square can be computed by below definition,

$$Nu_a = \frac{1/2S \oint_\Omega \alpha \partial T/\partial n}{\alpha/S(T_1 - T_2)} \tag{27}$$

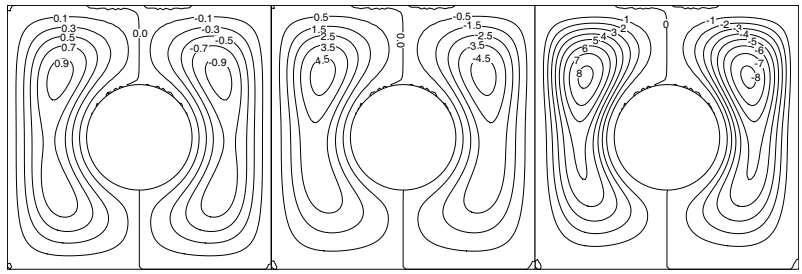

Fig. 7. Streamlines of nature convection in a concentric annulus at $Ra = 10^4$, 5×10^4, 10^5.

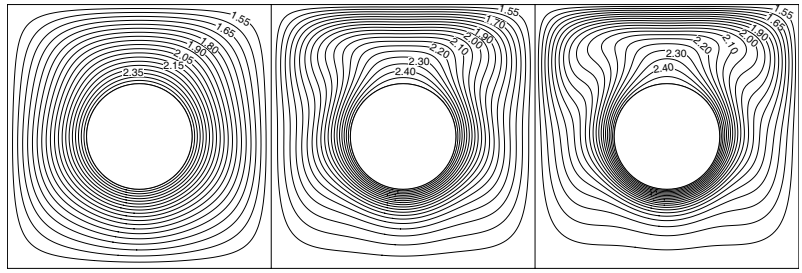

Fig. 8. Isotherms of nature convection in a concentric annulus at $Ra = 10^4$, 5×10^4, 10^5, the temperatures of inner cylinder and outer square are fix as 2.5, 1.5 respectively.

Table 4. The maximum stream function $\psi_{\max}$ and the average Nusselt number Nu_a.

	$\psi_{\max}$		Nu_a	
Ra	TLBE	Ref. 22	TLBE	Ref. 22
10^4	0.99	0.97	3.22	3.24
5×10^4	4.96	4.82	4.01	4.02
10^5	8.27	8.10	4.79	4.86

where T is the dimensional temperature, $\partial T/\partial n$ is the temperature gradient in the direction normal to the boundary. Ω is the boundary of inner or outer surface. S is the half length of corresponding boundary Ω. T_1, T_2 are the dimensional temperatures on the inner and outer walls respectively, α is the thermal conductivity. Here to avoid the difficulty of obtaining $\partial T/\partial n$ in the inner circular boundary, we calculated the Nu_a from the outer square boundary.

The numerical results of the maximum stream function $\psi_{\max}$ and the average Nusselt number Nu_a are shown in Table 4. The benchmark results using the DQ method[22] are also included for comparison. Good agreement between present results and the benchmark results further validates the thermal curved wall boundary treatment.

5. Conclusion

In this paper, a curved non-slip wall boundary treatment for isothermal Lattice Boltzmann equation (LBE)[13] was successfully extended to handle the thermal curved wall boundary for a double-population thermal lattice Boltzmann equation (TLBE). The unknown distribution population at a wall node which is necessary to fulfill streaming step is decomposed into its equilibrium and non-equilibrium parts.[13] The equilibrium part is evaluated according to Dirichlet and Neumann boundary constraints, and the non-equilibrium part is obtained using a first-order extrapolation from fluid lattices. The numerical simulation of Couette flow between two circular cylinders confirmed the thermal curved wall treatment is second-order accuracy. The results of natural convection in a square cavity, and the natural convection in a concentric annulus between an outer square cylinder and an inner circular cylinder all agree very well with available data in the literature. That further validated the thermal curved wall boundary treatment. Although the problems simulated here are all two-dimensional, this thermal curved wall boundary treatment can be applied to 3D thermal problems with complex geometry easily.

References

1. G. R. McNamara and G. Zanetti, *Phys. Rev. Lett.* **61**, 2332 (1988).
2. Y. H. Qian, D. d'Humières and P. Lallemand, *Europhys. Lett.* **17**, 479 (1992).
3. S. Chen and G. Doolen, *Annu. Rev. Fluid Mech.* **30**, 329 (1998).
4. S. Succi, *Lattice Boltzmann Equation for Fluid Dynamics and Beyond* (Clarendon Press, Oxford, 2001).
5. R. Cornubert, D. d'Humières and D. Levermore, *Physica D* **47**, 241 (1991).
6. D. P. Ziegler, *J. Stat. Phys.* **71**, 1171 (1993).
7. D. R. Noble, S. Chen, J. G. Georgiadis and R. O. Buckius, *Phys. Fluids* **7**, 203 (1995).
8. Q. Zou and X. He, *Phys. Fluids* **9**, 1591 (1997).
9. S. Chen, D. Martinez and R. Mei, *Phys. Fluids* **8**, 2527 (1996).
10. O. Filippova and D. Hänel, *J. Comput. Phys.* **147**, 219 (1998).
11. R. Mei, L. S. Luo and W. Shyy, *J. Comput. Phys.* **155**, 307 (1999).
12. M. Bouzidi, M. Firdouss and P. Lallemand, *Phys. Fluids* **13**, 3452 (2001).
13. Z. Guo, C. Zheng and B. Shi, *Phys. Fluids* **14**, 2007 (2002).
14. G. McNamara and B. Alder, *Physica A* **194**, 218 (1993).
15. X. Shan, *Phys. Rev. E* **55**, 2780 (1997).
16. X. He, S. Chen and G. D. Doolen, *J. Comput. Phys.* **146**, 282 (1998).
17. G. H. Tang, W. Q. Tao and Y. L. He, *Int. J. Mod. Phys. B* **17**, 183 (2003).
18. A. D' Orazio, S. Succi and C. Arrighetti, *Phys. Fluids* **15**, 2778 (2003).
19. T. Inamuro, M. Yoshino and F. Ogino, *Phys. Fluids* **7**, 2928 (1995).
20. G. H. Tang, W. Q. Tao and Y. L. He, *Phys. Rev. E* **72**, 016703 (2005).
21. C. Shu and H. Xue, *Int. J. Heat & Fluid Flow* **19**, 59 (1998).
22. C. Shu and Y. D. Zhu, *Int. J. Numer. Meth. Fluids* **38**, 429 (2002).
23. Y. Peng, C. Shu, Y. T. Chew and T. Inamuro, *Phys. Rev. E* **69**, 016703 (2004).